24th COBEM - 2017

24th ABCM International Congress of Mechanical Engineering
December 3-8, 2017, Curitiba, PR, Brazil

COBEM-2017-2271
HYBRID BIPOLAR STEPPER MOTOR CONTROL BY VARIABLE GAIN PID CONTROLLER

Iago Camargo Silveira
Rafael Antônio Comparsi Laranja
Universidade Federal do Rio Grande do Sul, Mechanical Engineering Department, Porto Alegre, Brazil
Email: iagocamargosilveira@gmail.com. Email: rafael.laranja@ufrgs.br

Abstract. *Stepper motors are used in tasks that require positioning accuracy and trajectory tracking, such as CNC machines and robotic manipulators. Several studies show the use of the PID strategy to control this type of motor, as well as the need to modify this type of control due to nonlinearities and the possibility of instability. Due to these problems, this article proposes a variable gain PID control algorithm, where gains are found based on the allocation of the desired dynamics poles, according to the possible peak time and the specified damping coefficient. The first is found by the instantaneous accelerations that can be developed by the motor due to the variation of the torque according to the instantaneous speed of operation, that is, by the map of the stepper motor. Lyapunov stability theory is used to prove the large-scale asymptotic stability of the proposed control, by limiting control gains. Simulations of the proposed control with respect to its parameters and the motor operating variables are presented, presenting agreement with the allowable for operation of the simulated actuator. In addition, the proposed control is compared with a fixed gains PID control, showing better results for the point-to-point movement simulations and trajectory tracking, with a reduction of 87.5% of the error dimension in trajectory tracking.*

Keywords: *Stepper motors; Varied gain PID controller; Lyapunov stability theory;*

1. INTRODUCTION

Stepper motors are interesting alternatives to open loop control, due to the discretization of their incremental movement and consequent ease of control for this operation. However, some problems arise for this type of arrangement, of which, it is mentioned the low performance possible to be developed by the actuator, due to the possibility of loss of steps and the instability, which is improved considerably in closed loop, as shown by Cao et al, 1998.

One of the main causes of step loss, also known as loss of synchronism, according to Acarnley, 2002, occurs when the torque demanded for the motor is higher than its capacity of torque at that operation speed, whereas the torque varies inversely with the operation speed.

Due to these problems and control tendencies presented for this type of actuator, which will be presented in Chapter 3, it is proposed a control algorithm to which the values of the PID control gains vary at each processing step, due to the non-linearities of the motor and its capacity of performance. The proposed control was carried out based on the mathematical modeling of a bipolar two step hybrid motor.

2. MATHEMATICAL MODELING

The focus of this chapter is to present the mathematical modeling, which will base the design of the controller and the computational simulations performed. To do so, it begins by addressing the dynamics regarding the electrical and the mechanical subsystem of the actuator.

2.1 Electrical Subsystem

This subsystem is divided into two parts: The first one is related to the electric system that represents it, which is interconnected with the dynamics of the actuator movement (mechanical part) through an electromagnetic torque coming from the actuator, being the second part of this subsystem.

The mathematical modeling of the actuator electric circuit is found from Figure 1, exemplified for phase A of the stepper motor, in which, Equations 1 and 2 represent the electrical dynamics of phases A and B, respectively.

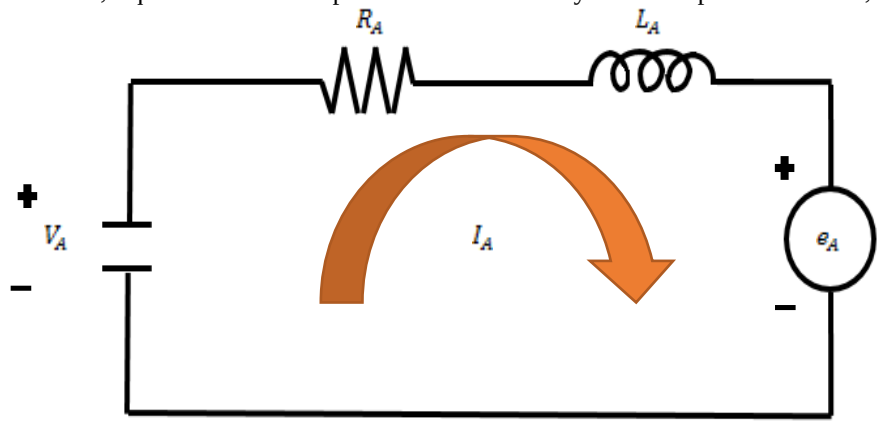

Figure 1 – Stepper motor circuit exemplified for phase A.

$$V_A = R_A I_A + L_A \frac{dI_A}{dt} - e_A \tag{1}$$

$$V_B = R_B I_B + L_B \frac{dI_B}{dt} - e_B \tag{2}$$

where $V_{A,B}$ is the supply voltage, $R_{A,B}$ is the electrical resistance, $I_{A,B}$ is the electrical current, $L_{A,B}$ is the electrical inductance, $e_{A,B}$ is the induced voltage, in each of the phases.

For a two-phase stepper motor, the flux induced by the interaction between the permanent magnet of its rotor and the coil of the stator phases is found by Equations 3 and 4 for phases A and B:

$$\varphi_A = \varphi_M \cos(p\theta) \tag{3}$$

$$\varphi_B = \varphi_M \cos(p\theta - {}^{\pi}/_{2}) \tag{4}$$

where φ_A and φ_B are the induced flows in phases A and B, φ_M is the maximum induced flow, p is the motor phase pairs number, and θ é is the angle of rotation of the actuator rotor.

These voltages induced by this flow are found by Equations 5 and 6 for phases A and B:

$$e_A = \frac{d\varphi_A}{dt} = -p\varphi_M \dot{\theta} \sin(p\theta) \tag{5}$$

$$e_B = \frac{d\varphi_B}{dt} = -p\varphi_M \dot{\theta} \sin(p\theta - {}^{\pi}/_{2}) \tag{6}$$

where $\dot{\theta}$ is the speed of rotation of the rotor actuator. Based on Equations 5 and 6, Equations 1 and 2 can be changed, as shown in Equations 7 and 8:

$$V_A = R_A I_A + L_A \frac{dI_A}{dt} - p\varphi_M \dot{\theta} \sin(p\theta) \tag{7}$$

$$V_B = R_B I_B + L_B \frac{dI_B}{dt} - p\varphi_M \dot{\theta} \sin(p\theta - {}^{\pi}/_{2}) \tag{8}$$

Equations 7 and 8 show the dynamic behavior of the electrical circuit representative of the subsystem, for phases A and B. It should be mentioned that this mathematical modeling is shown in several studies, which are indicated Kabde et al., 2014, Elksasy et al, 2010 , Baldha et al, 2015, Kamalasadan, 2007, Cardozo, 2012, as they will be reviewed later.

The electromagnetic torque provided by the motor phases A and B are shown by Equations 9 and 10:

$$T_A = -p\varphi_M I_A \sin(p\theta) \tag{9}$$

$$T_B = -p\varphi_M I_B \sin(p\theta - {}^{\pi}/_{2}) \tag{10}$$

where T_A e T_B are electromagnetic torque provided by the motor phases A and B.

Mayé, 2016, simplifies these equations by grouping Equations 9 and 10, which together provide the electromagnetic torque of the motor, in the case of a power supply by a bipolar driver in a two phases bipolar stepper motor, as the controller design is carried out, thus $I_A = I_B = I$ and the electromagnetic torque of the motor can be found by Equation 11:

$$T_M = \varphi_M I\sqrt{2} \sin(\theta - {}^{\pi}/_{4}) \tag{11}$$

where T_M is the electromagnetic torque of the motor

Following the same logic of Mayé, 2016, for the electromagnetic torque of the motor, an equivalent electrical system is realized for the two phases of the actuator, in order to be able to group Equations 1 and 2. The equivalent electrical system is shown in Figure 2:

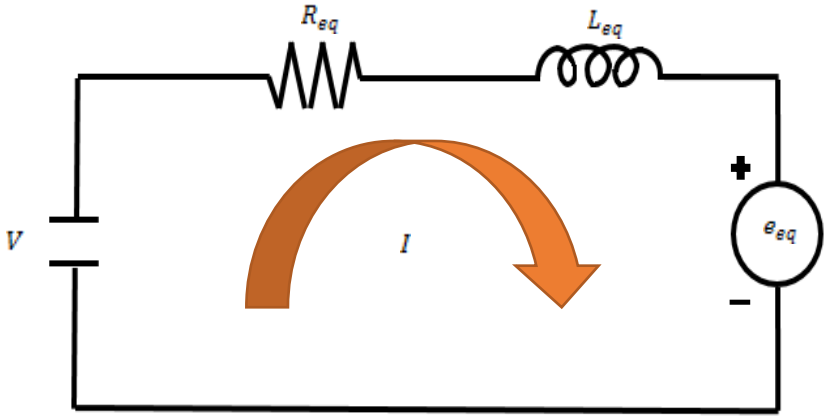

Figure 2 – Equivalent electrical circuit for a two-phase stepper motor

The mathematical modeling of the electrical circuit in Figure 2 is shown in Equations 12, which is the grouping of the terms of Equations 1 and 2:

$$V = R_{eq} I + L_{eq} \frac{dI}{dt} - e_{eq} \tag{12}$$

where R_{eq} and L_{eq} are the equivalent electrical resistance and inductance of the grouping of phases A and B, which depend on the phase connection (series or parallel), e_{eq} is the equivalent induced voltage to the grouping of phases A and B.

Equivalent induced voltage can be found in a manner similar to what Mayé, 2016, did for the electromagnetic torques of phases A and B. For this reason, joining the last terms Equations 7 and 8, we arrive at Equations 13, referring to equivalent voltage induced:

$$e_{eq} = -\varphi_M \dot{\theta}\sqrt{2} \sin(\theta - {}^{\pi}/_{4}) \tag{13}$$

Based on this, Equations 12 can be modified. This change is shown in Equations 14, which results in the final equation for the electrical circuit dynamics for the bipolar stepper motor:

$$V = R_{eq} I + L_{eq} \frac{dI}{dt} + \varphi_M \dot{\theta}\sqrt{2} \sin(\theta - {}^{\pi}/_{4}) \tag{14}$$

Finally, in addition to the electromagnetic torque, the stepper motors produce a torque induced by the interaction of the permanent magnet of the stator with the phase coils. This torque is contrary to the electromagnetic torque, which is called retention torque. According to Mayé, 2016, the retention torque is found by Equations 15:

$$T_r = t_r \sin(4\theta) \tag{15}$$

where T_r is the retention torque and t_r is the maximum value of the retention torque.

2.2 Mechanical Subsystem

This subsystem is usually divided by its components according to what they represent. A term referring to the inertia of the system, one or more terms related to the friction and a component relative to the torque requested by the motor can be commonly seen representing this subsystem.

Based on the models used mainly in stepper motor papers (Kabde et al, 2014, Elksasy et al, 2010, Baldha et al, 2015, Kamalasadan, 2007, Cardozo, 2012) and lack of experiments to find a model of friction more elaborate and consistent with reality, a mathematical model with only the viscous component of the friction is used. Equation 16 presents this model:

$$T_{Mec} = J\frac{d^2\theta}{dt^2} + C_f\frac{d\theta}{dt} + T_c \tag{16}$$

where T_{Mec} is the mechanical torque that requests the actuator, J is the inertia associated to the motor, C_f is the friction term relative to the viscous friction, T_c it is the torque that requests the actuator.

3. CONTROLLER DESIGN

Based on the control problems presented in the introduction of this paper, we have studied some articles involving the control of stepper motors to find out the ways to control this type of actuator.

Elksasy et al., 2010, uses a PID control modified by an open loop gain factor to stabilize the stepper motor control. The results of his study are compared with the PID without this modification, showing better results, especially when the stepper motor was excited with some disturbance.

Cardozo, 2012, proposes an integral proportional control algorithm with maximum and minimum speed limitations per controller processing cycle based on maximum motor acceleration without loss of steps. In this way, the control proposed by the author controls the frequency of actuator steps.

Kabde et al., 2014, applies fuzzy logic in conjunction with the PID control to control the stepper motor in point-to-point moviment, showing better results when compared to the PID control, especially with respect to the startling to reach the required position.

Kamalasadan, 2007, used the technique of neural networks in parallel with PID control for the trajectory tracking simulation and point-to-point movement, showing smaller errors with this technique, compared to the PID control.

According to Carrillo-Serrano et al., 2014, the most adopted control strategy in practice is the derivative proportional control, where the input variable, to be controlled, is the electrical current, through the switching between the phases of the stepper motor, where the electrical current is controlled based on the torque required by the modeled mechanical part. Moreover, the dynamics regarding the electrical part is negligence in this type of control.

As can be seen in these studies, the PID control strategy is adopted for this type of motor, but it does not present such satisfactory results, which makes the researchers use several techniques to, together with this strategy, to adjust the control and, consequently, accuracy and stability of the actuator. Based on this, a PID pole relocation strategy was initially adopted to make the controller design for the actuator.

3.1 PID Controller with Varied Gains

The control design, starts from the mathematical modeling shown in the previous chapter, equating the torque produced by the stepper motor to the mechanical torque coupled to it, presented in Equation 17.

$$J\frac{d^2\theta}{dt^2} + C_f\frac{d\theta}{dt} + T_c = \varphi_M I\sqrt{2}\,\mathrm{sen}\left(\theta - {}^{\pi}/_{4}\right) - t_r\,\mathrm{sen}(4\theta) \tag{17}$$

To find the transfer function of this system, the Equation 17 must be linearized and transform it into the frequency domain. As can be seen in this equation, the two terms on the right side of equality are non-linear and the first term depends on two variables. In this way, this term must be linearized with respect to the electrical current and with respect to the rotor position. Equations 18, 19 and 20 present the derivatives of each term for the linearization process.

$$\frac{\partial T_e}{\partial I} = \varphi_M\sqrt{2}\,\mathrm{sen}\left(\theta^* - {}^{\pi}/_{4}\right) \tag{18}$$

$$\frac{\partial T_e}{\partial \theta} = \varphi_M I^* \sqrt{2} \cos\left(\theta - {}^{\pi}/_{4}\right) \tag{19}$$

$$\frac{\partial T_r}{\partial \theta} = 4t_r \cos(4\theta^*) \tag{20}$$

where $\frac{\partial T_e}{\partial I}$ is the derivative of the electromagnetic torque of the actuator with respect to the electrical current I, $\frac{\partial T_e}{\partial \theta}$ is the derivative of the electromagnetic torque of the actuator with respect to the position of the motor rotor θ, $\frac{\partial T_r}{\partial \theta}$ is the derivative of the retention torque with respect to the position of the motor rotor.

Based on the linearized terms, Equation 21 shows the linearization of Equation 17.

$$J\frac{d^2\theta}{dt^2} + C_f\frac{d^2\theta}{dt^2} = \varphi_M \sqrt{2}\,\mathrm{sen}\left(\theta^* - {}^{\pi}/_{4}\right)\Delta I + \varphi_M I^* \sqrt{2}\cos\left(\theta - {}^{\pi}/_{4}\right)\Delta\theta - 4t_r\cos(4\theta^*)\Delta\theta \tag{21}$$

Analyzing Equation 21, the most intuitive quantity to be controlled is the electrical current, and, as shown above, this is the quantity most commonly used to control this type of actuator.

Equation 21 is transformed into the frequency domain, resulting in Equation 22.

$$Js^2\theta(s) + C_f s\theta(s) = \varphi_M \sqrt{2}\,\mathrm{sen}\left(\theta^* - {}^{\pi}/_{4}\right) I(s) + \varphi_M I^* \sqrt{2}\cos\left(\theta - {}^{\pi}/_{4}\right)\theta(s) - 4t_r\cos(4\theta^*)\,\theta(s) \tag{22}$$

All terms of Equation 22 are divided by inertia J and the equals terms are grouped, resulting in Equation 23.

$$\left(\frac{\varphi_M \sqrt{2}\,\mathrm{sen}\left(\theta^* - {}^{\pi}/_{4}\right)}{J}\right) I(s) = \left(s^2 + \frac{C_f}{J}s\ \frac{-\varphi_M I^* \sqrt{2}\cos\left(\theta - {}^{\pi}/_{4}\right)\theta(s) + 4t_r\cos(4\theta^*)}{J}\right)\theta(s) \tag{23}$$

Based on Equation 23, we can find the transfer function of this system, but for the simplification of this step, the terms of this Equation are grouped, according to Equation 24, 25 and 26.

$$A = \frac{\varphi_M \sqrt{2}\,\mathrm{sen}\left(\theta^* - {}^{\pi}/_{4}\right)}{J} \tag{24}$$

$$B = \frac{C_f}{J} \tag{25}$$

$$C = \frac{-\varphi_M I^* \sqrt{2}\cos\left(\theta - {}^{\pi}/_{4}\right)\theta(s) + 4t_r\cos(4\theta^*)}{J} \tag{26}$$

In this way, the transfer function can be assembled, being presented in Equation 27.

$$\frac{\theta(s)}{I(s)} = \frac{A}{s^2 + Bs + C} = G(s) \tag{27}$$

where $G(s)$ is the open-loop transfer function.

Before starting the closed-loop transfer function, it is usual in control techniques for electrical motors, that the control signal is not directly the electrical current, but that this signal is multiplied by a gain to become the current to the electrical actuator, as presented by Equation 28:

$$I = K_i u \tag{28}$$

where K_i is gain that transforms the control signal into the electrical current and u is the control signal.

For the closed-loop PID control, Equation 29 shows the system gains multiplied by their respective terms in the frequency domain.

$$H(s) = \frac{K_a s^2 + K_v s + K_p}{s} \tag{29}$$

The closed-loop transfer function is obtained by Equation 30:

$$T(s) = \frac{G(s)}{1 + G(s)H(s)} \tag{30}$$

Figure 3 represents the state feedback control scheme (position, velocity and acceleration), exemplified for point-to-point movement, and the previously presented functions can be observed.

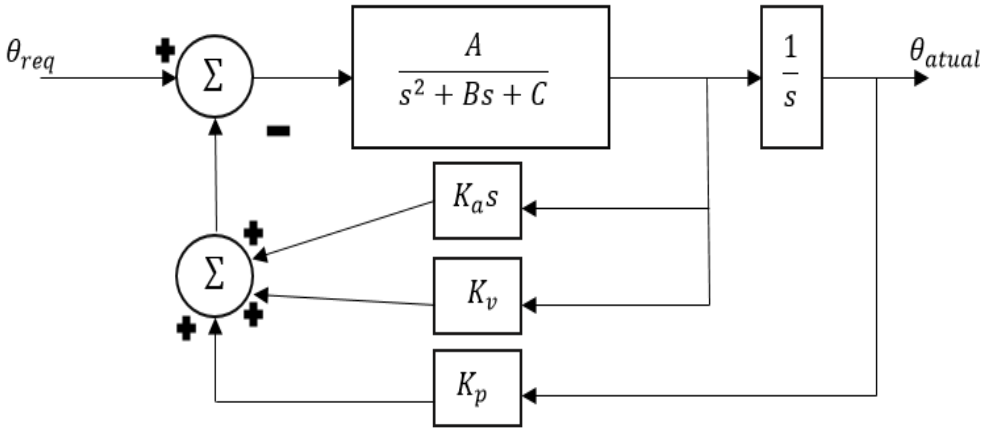

Figure 3 – State feedback control scheme (PVA) exemplified for point-to-point moviment

In Figure 3, θ_{req} is the required position to the actuator rotor and θ_{atual} is the current position of the actuator rotor. The simplified, closed loop transfer function of the system is found by applying Equations 27, 28 and 29 in Equation 30, and it is demonstrated, after some simplifications, by Equation 31:

$$T(s) = K_i \left(\frac{As}{s^3 + (K_a A + B)s^2 + (K_v A + C)s + (K_p A)} \right) \tag{31}$$

According to Ogata, 1997, one of the ways to find the gains of the PID control for the desired pole reallocation is based on the discovery of the closed-loop transfer function that characterizes the dynamic system (Equation 31) and compare it with a equation, from which, its coefficients are calculated according to the desired dynamics of the system to be controlled.

Based on this comparison, it is possible to determine the values of the gains needed to achieve the desired dynamics. Equation 32 shows a third order system with the coefficients found according to the desired dynamics.

$$s^3 + A_1 s^2 + A_2 s + A_3 \tag{32}$$

where A_1, A_2 and A_3 are the coefficients of the desired dynamics equation for the system.

By comparison, we obtain the values required for the system gains, represented by Equations 33, 34 and 35, for the acceleration, velocity and position gain, respectively.

$$K_a = \frac{A_1 - B}{A} \tag{34}$$

$$K_v = \frac{A_2 - C}{A} \tag{35}$$

$$K_p = \frac{A_3}{A} \tag{36}$$

Two questions arise from the analysis of the system gains equations. The first is relative to the coefficients of the linearized equation of the system. The terms A and C are oscillatory because they derive from the sine of the dynamic

equation of the system. Thus, the use of fixed values for A and C, for the adjustment of gains would result in a very narrow range to which these gains would be ideal for the desired dynamics.

It is concluded that due to the needs of the project, the control should be able to recalculate the values of A and C *in* each processing step, and consequently the values of the gains to suit the new motor conditions.

The second fact is relative to the choice of the parameters that will be considered for the determination of the dynamics required to the system. Ogata, 1997, presents several parameters that can be chosen according to the project. Figure 4 shows some of the parameters that can be used to find the desired dynamics.

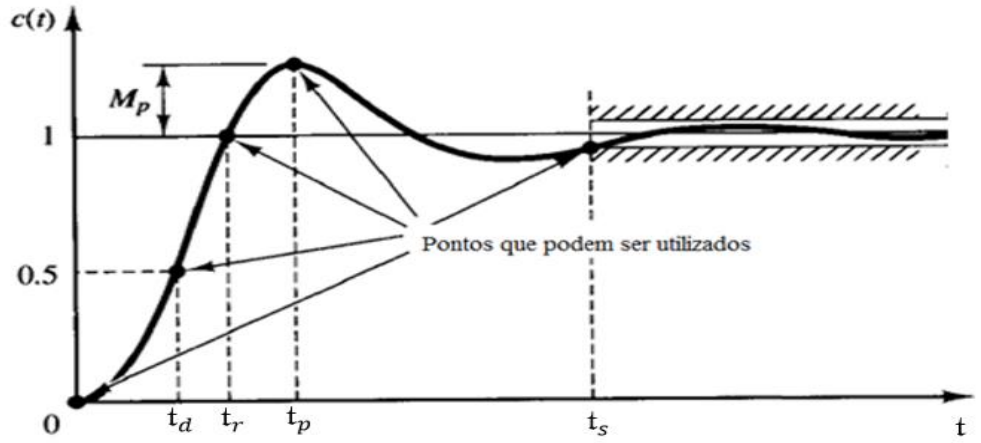

Figure 4 – Possible parameters to be used to find the desired dynamics of the control system. Adapted from Ogata, 1997.

In Figure 4, t is the time, t_d is the delay time, corresponding to 50% of the value of the point aimed at to be reached by the system, t_r is the rise time, that is, the time necessary to reach the desired position. t_p is the peak time, corresponds to the time required to reach the required position plus the startling, M_p, relative to that position, t_s is the stabilization time of the controlled system relative to the oscillation around the estimated point.

Based on this, and in the problems regarding the control of step motors, previously presented, it was conceived that the most adequate parameters to determine the values of the coefficients of the dynamics required to the system are the pike time, t_p, and the damping coefficient, ε, of the system .

As previously mentioned, in order to the control to be able to perform its function adequately, it is necessary that the values of the gains be recalculated at each processing step. Thus, the peak time used to generate the coefficients of the desired dynamics can also be recalculated at each processing step to calculate which coefficient values are ideal for the momentary operating conditions.

The peak time was chosen because it is the largest time parameter that can be used to find the system desired dynamics, relative to reach the required position, since it is related to the initial position and the maximum position reached by the actuator.

In addition, this parameter can be used as the time, at which, from the momentary position and velocity conditions and acceleration possible to be developed by the motor, it is possible to determine the value of this parameter. Therefore, it is justified to choose this parameter, since it is a more conservative term, guaranteeing that the gains calculated from it will not direct the loss of steps by the actuator.

Based on this, a second order equation that calculates the possible peak time value, due to the conditions of actuation, is presented by Equation 37.

$$t_p = -\frac{2\dot{\theta}_o}{\ddot{\theta}_{pos}} \mp \sqrt{\left(\left(\frac{2\dot{\theta}_o}{\ddot{\theta}_{pos}}\right)^2 + \frac{4\Delta\theta}{\ddot{\theta}_{pos}}\right)} \tag{37}$$

where $\dot{\theta}_o$ is the instantaneous speed of operation, $\ddot{\theta}_{pos}$ is the possible acceleration to be developed, $\Delta\theta$ is the difference between the required position and the momentary position.

The possible acceleration to be developed by the actuator was chosen to calculate the value of the peak time, in front of the instantaneous acceleration of the motor, because this parameter ensure that the loss of steps does not happen, as it limits the operation to the possible actuator condition. In addition, this parameter can be calculated, at each processing step, from the motor map.

The motor map consists of the relationship between the available torque capacity of the actuator relative to the operation speed. Figure 5 shows an example of this relationship for the stepper motor used in this paper (Akiyama, 2008).

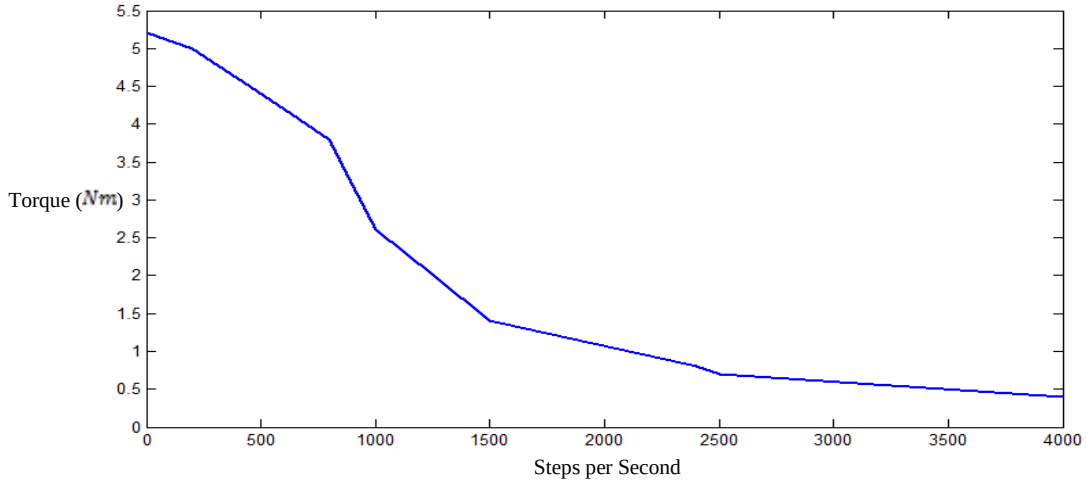

Figure 5 – Relation between torque capacity and stepper motor speed. Adapted from Akiyama, 2008.

Thus, having as input parameters the operating speed, the maximum possible torque for this condition is found. That way, the acceleration possible to be developed can be found by Equation 37.

$$\ddot{\theta}_{pos} = \frac{T_{disp}}{J} \tag{37}$$

where T_{disp} is the available torque.

Thus, the possible peak time for the operation is calculated, being chosen, between the two values available by Equation 37, the lowest positive.

The parameters to find the desired dynamic is complete with a damping coefficient (ε) of 0,8.

Based on this, through Equation 38 the natural frequency of the desired system is found.

$$\omega_n = \frac{\pi}{t_p\sqrt{1-\varepsilon^2}} \tag{38}$$

The natural frequency of the system is used to find the poles of the desired third-order dynamics. Equation 39 presents the way to find the first two poles, while Equation 40 presents for the third pole, as was used in Allgayer, 2011.

$$P_{1,2} = -\varepsilon\omega_n \mp \omega_n\sqrt{\varepsilon^2-1} \tag{39}$$

$$P_3 = -10\varepsilon\omega_n \tag{40}$$

From the poles of the system, it is possible to calculate the coefficients of the third-order dynamics required for the system. Equations 41, 42 and 43 present this step.

$$A_1 = -(P_1 + P_2 + P_3) \tag{41}$$

$$A_2 = P_1P_2 + P_1P_3 + P_2P_3 \tag{42}$$

$$A_3 = P_1P_2P_3 \tag{43}$$

With the result of these equations, we can apply these values in Equations 34, 35 and 36 and find, respectively, the values of the gains K_a, K_v and K_p, which guarantee the desired dynamics to the controlled stepper motor. For the best understanding, the flowchart of Figure 6 shows the proposed control algorithm.

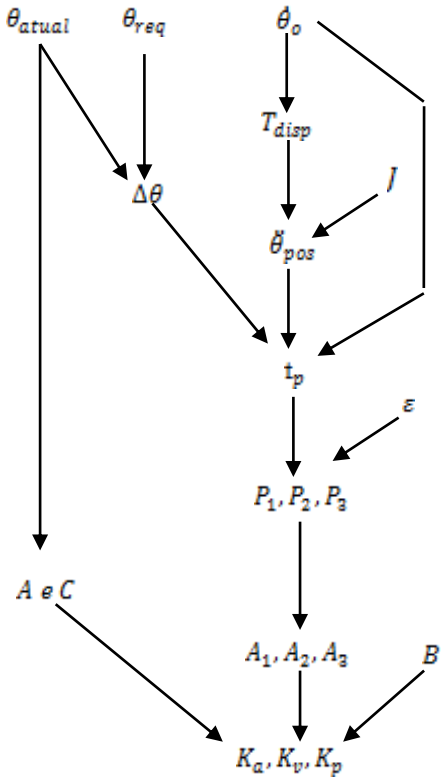

Figure 6 – Flowchart of the proposed control algorithm.

It is noticed that the parameters of the system needed for the control algorithm are the position and the current speed, and these parameters must already be measured along the operation due to the proposed control, that requires the position, velocity and acceleration error (PVA controller) to find the control signal for the actuator.

3.2 Control Stability

As previously shown, one of the problems of stepper motor control is the possible instability of the system. Based on this, we have studied ways of demonstrating the stability of this control systems.

According to Ogata, 1997, for nonlinear control systems the most widespread way of proving the stability of these systems is through the Lyapunov stability criteria. Also, according to Ogata, 1997, there are some methods to prove, through the stability theory of Lyapunov, the stability of the system, one of which is through the so-called Lyapunov function.

This function is chosen or determined from the control system state space, functioning as an energy function, from a mechanical system, to the control system analyzed.

Thus, if this function has a tendency to decrease its value over time, the stability of the system is proven, since a mechanical system (mass, spring and damper) that decreases its energy over time is stable. A function that fulfills this requirement is said to be defined negatively. Equation 44 presents this requirement.

$$\dot{\mathcal{L}}(x,t) < 0 \tag{44}$$

where $\mathcal{L}(x,t)$ is the Lyapunov funcion and $\dot{\mathcal{L}}(x,t)$ is the time derivative of this function.

In addition, to ensure that a point of stability remains on a surface of the state space it is necessary that the inequality of Equation 45 be obeyed.

$$\mathcal{L}(x,t) > 0 \tag{45}$$

A function that fulfills this requirement is said positively defined. In addition, the fulfillment of this requirement, covering the entire space of states ($x \to \infty$), imposes that the chosen Lyapunov function is stable throughout all the extension of state space.

Thus, if the chosen Lyapunov function, to represent the hypothetical energy function of the system, obeys the stability requirements imposed by these criterions, the system to be controlled is said to be asymptotically stable in the Lyapunov sense and if it covers the entire state space, this is said to be asymptotically stable in the large sense of Lyapunov.

Based on this, some papers that deal with this subject were studied. Machin, 2017, proposes a Lyapunov function for the controlled system, and shows that the controlled system is asymptotically stable according to previously established criteria for the control, as well as Borges, 2017, which also uses limitations of system gains to ensure that it is stable in the Lyapunov sense.

Rachid, 2006, uses the Lyapunov criterion to find the stepping motor control laws to guarantee the stability of the control system, thus, as Borges, 2017, finds the inequalities, among the controllable parameters, necessary to guarantee stable control.

Following these criteria and based on the presented works, a Lyapunov function for the system is proposed, indicated by Equation 46:

$$\mathcal{L}(x,t) = \frac{I^2}{2} \tag{46}$$

As can be seen, this function is always positive, regardless of the value of the electrical current supplied to the actuator. In this way, the Lyapunov function of the system is defined positively.

The chosen function is based on the state space of the system, as shown by the control law in Equation 47.

$$I = K_i\left(K_a\ddot{\theta} + K_v\dot{\theta} + K_p\theta\right) \tag{47}$$

where $\ddot{\theta}$, $\dot{\theta}$ and θ represent the acceleration, velocity and position error of the system, respectively. For this study, stability has been taken into account from the origin of the system, that is, the starting point is zero. In this way, Equation 47 is transformed, as presented in Equation 48:

$$I = K_i\left(K_a\ddot{\theta} + K_v\dot{\theta} + K_p\theta\right) \tag{48}$$

Thus, we can also analyze that Equation 48 tends to infinity when state variables tend to infinity. Thus, if the second stability criterion has been proved, the system can be said to be stable asymptotically in the large sense of Lyapunov. Applying the criterion imposed by Equation 44 in Equation 46, we have Equation 49.

$$\dot{\mathcal{L}}(x,t) = I\frac{dI}{dt} < 0 \tag{49}$$

The time derivative of the electrical current (dI/dt) can be found based on Equation 14, being shown in Equation 50.

$$\frac{dI}{dt} = \frac{1}{L_{eq}}\left(V - R_{eq}I - \varphi_M\dot{\theta}\sqrt{2}\,\mathrm{sen}\left(\theta - {}^{\pi}/_{4}\right)\right) \tag{50}$$

Applying Equation 50 in Equation 49, we arrive at Equation 51, after grouping the terms.

$$\dot{\mathcal{L}}(x,t) = \frac{IV}{L_{eq}} - \frac{R_{eq}I^2}{L_{eq}} - \frac{\varphi_M I\dot{\theta}\sqrt{2}\,\mathrm{sen}\left(\theta - {}^{\pi}/_{4}\right)}{L_{eq}} < 0 \tag{51}$$

The last term of Equation 51 is analyzed, applying the control law presented in Equation 48, where the gains are replaced according to Equations 34, 35 and 36. This analysis is presented in Equation 52.

$$\frac{K_i\left((A_1 - B)\ddot{\theta} + (A_2 - C)\dot{\theta} + (A_3)\theta\right)}{A}\,\frac{\varphi_M\dot{\theta}\sqrt{2}\,\mathrm{sen}\left(\theta - {}^{\pi}/_{4}\right)}{L_{eq}} \tag{52}$$

The value of A is replaced by the result in Equation 24, being applied in Equation 52, resulting in Equation 53:

$$\frac{\varphi_M K_i \dot{\theta}\sqrt{2}}{L_{eq}} \frac{(A_1 - B)\ddot{\theta} + (A_2 - C)\dot{\theta} + (A_3)\theta}{\left(\frac{\varphi_M}{J}\sqrt{2}\right)} \frac{\text{sen}\left(\theta - {}^{\pi}/_{4}\right)}{\text{sen}\left(\theta - {}^{\pi}/_{4}\right)} \tag{53}$$

Applying the possible simplifications, this term is reduced, as presented in Equation 54:

$$\frac{JK_i\dot{\theta}\left[(A_1 - B)\ddot{\theta} + (A_2 - C)\dot{\theta} + (A_3)\theta\right]}{L_{eq}} \tag{54}$$

After these simplification operations, Equation 51 is rearranged, as shown in Equation 55:

$$\frac{I}{L_{eq}}\left[\frac{V - R_{eq}I}{L_{eq}}\right] - \frac{K_i\dot{\theta}J\left[(A_1 - B)\ddot{\theta} + (A_2 - C)\dot{\theta} + (A_3)\theta\right]}{L_{eq}} < 0 \tag{55}$$

Applying, again, the control law of Equation 48, we arrive at Equation 56:

$$K_i\left(K_a\ddot{\theta} + K_v\dot{\theta} + K_p\theta\right)\left[\frac{V - R_{eq}I}{L_{eq}}\right] < \frac{K_i\dot{\theta}J\left[(A_1 - B)\ddot{\theta} + (A_2 - C)\dot{\theta} + (A_3)\theta\right]}{L_{eq}} \tag{56}$$

As shown previously, some studies that use the Lyapunov requirements to prove the stability of their systems, use these criteria required to find limits for their control parameters.

Based on that, and in the result of the simplifications presented in Equation 56, the equals terms are joined by means of the inequality presented in this equation and, in this way, it shows the arrives at the limits for the gains of the control system, presented, respectively, by Equations 57, 58 and 59, which ensure that the designed control system is asymptotically stable on a large scale.

$$K_a < \frac{\dot{\theta}J[(A_1 - B)]}{V - R_{eq}I} \tag{57}$$

$$K_v < \frac{\dot{\theta}J[(A_2 - C)]}{V - R_{eq}I} \tag{58}$$

$$K_p < \frac{\dot{\theta}JA_3}{V - R_{eq}I} \tag{59}$$

Analyzing the results of Equations 57, 58 and 59, it can be seen that the operating limits of control system gains depend on operating parameters ($\dot{\theta}, A_1, A_2, A_3, B\ e\ C$), as well as on electrical parameters of the system ($V, I\ e\ R_{eq}$), which is interesting due to the lack of modeling of the electrical dynamics for the controller design. However, it is noticed that several of the equations terms are variable throughout the operation, in this way, this limitation is variable throughout the operation.

In addition, it is proven the necessity of these limits, because as can be seen, by the analysis of Equations 34, 35 and 36, the gains of the system are calculated from a division of a senoid (term A), which causes, in each crossing the zero of this sonoide, that the values of the gains tend to infinity. Thus, it is necessary to have a limitation for these gains, so that the electrical current, coming from the control signal, does not exceed admissible values for operation.

4. SIMULATIONS AND RESULTS

In this chapter, the simulations for the stepper motor will be presented, focusing on its variables and control parameters presented in the previous chapter. After this simulation, we will show the results of the simulation of this control algorithm compared to a PID control with fixed gains in a stepper motor for the trajectory tracking tests and the point-to-point movement.

All simulations of this chapter were carried out in the simulation environment of MatLab, simulink. Relative and absolute error were set at $1 * 10^{-14}$. The processing step was established with a minimum value of $1 * 10^{-3}s$ and maximum of $1 * 10^{-6}s$.

The parameters of the electrical actuators required for the simulation are shown in Table 1.

Table 1 – Parameters of the electric actuator for the simulations

Parameters	Values
$T_{máx}$	5,55 Nm
φ_M	0,4 Vs
t_r	0,26 Nm
J	0,02 $kg\,m^2$
C_f	0,05 $kg\ m/s$

In addition to these parameters, as presented in the last section of the previous chapter, system gains are limited by the Lyapunov stability theorem. As shown in Equations 57, 58 and 59, most of the terms used to limit the gains are variable throughout the operation, but some of these terms must be assumed constant, such as electrical current and voltage. These parameters must be assumed constant because their measurement was not designed by the PVA controller, besides the practical problem that would be to add two more variables to be monitored. Thus, we assume the constant values presented in Table 2 for the electrical current, voltage and equivalent electric resistance.

Table 2 – Constant Parameters for Gain Limits

Variables	Used Values
Electrical Current	0,1 A
Voltage	3,75 V
Equivalent electrical resistance	0,375 Ω

The values of the voltage and the equivalent electrical resistance of the phases, presented in Table 2, were calculated according to the stepper motor manual (Akiyama, 2008) studied for the simulation, according to a series connection of the actuator phases. The electrical current was assumed with a minimum value so that the gain limit was maximized.

4.1 Stepper motor with the proposed control

In this initial part, we discussed the control presented for the stepper motor and also the behavior of the parameters of this actuator during the operation.

Point-to-point movement requires more torque and power developed by the actuator, because this type of motion does not require an acceleration limit, as it does for trajectory tracking. Due to the greater demand for the motor and consequently the greater need of control to guarantee stability and that the limits of the proper performance are respected, this simulation will show the behavior of parameters of the control, besides the variables of the motor, for a point-to-point movement.

The simulations were performed in the simulation environment of MatLab, the simulink, as previously mentioned, using a simulation time of 6.5 seconds, since this is the time that can be perceive the stabilization of the motor in the required position, with speed and acceleration errors minimized, as will be shown later. Figure 7 shows the movement of the simulation, being chosen for the motor to start the operation of the zero point and reach the point corresponding to 100 radians.

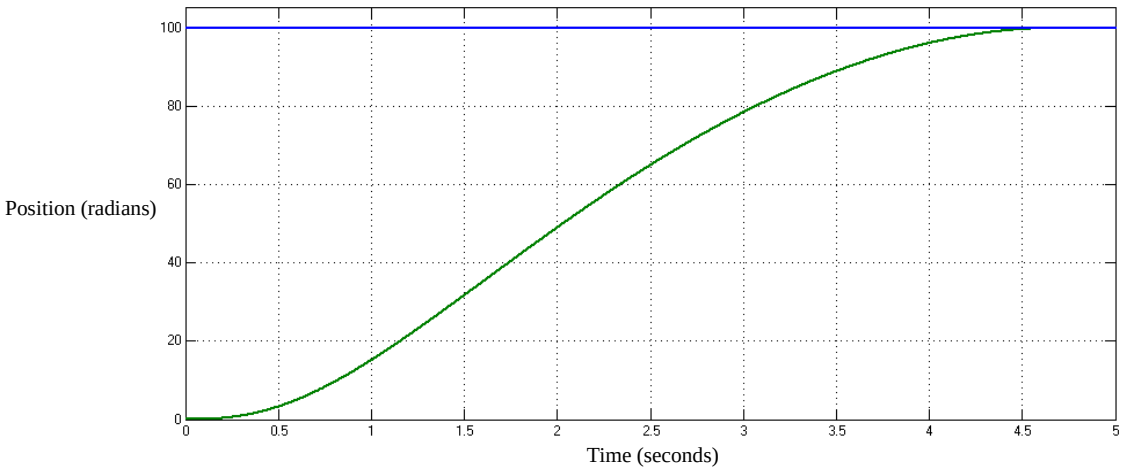

Figure 7 – Point-to-point simulation for motor control test

As shown in the previous chapter, the first step of the control is to calculate, by means of the developed speed and the motor map, which acceleration is possible to be developed. Figure 8 shows the possible acceleration to be developed by the actuator.

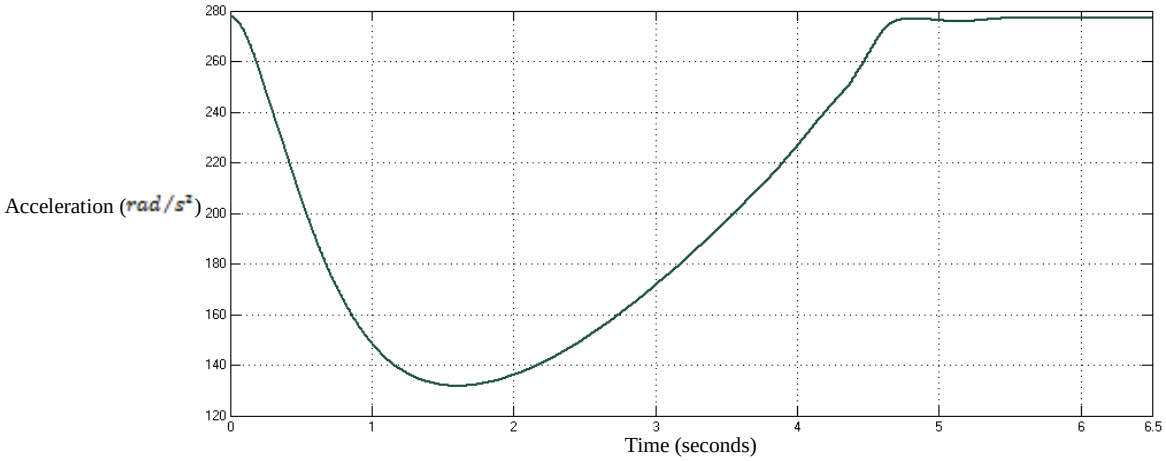

Figure 8 – Acceleration possible to be developed by the actuator

With this parameter determined continuously, and with the reading of the developed speed and the position reached by the actuator, it is able to determine the peak time necessary to determine the parameters of the desired dynamics, which is shown in Figure 9.

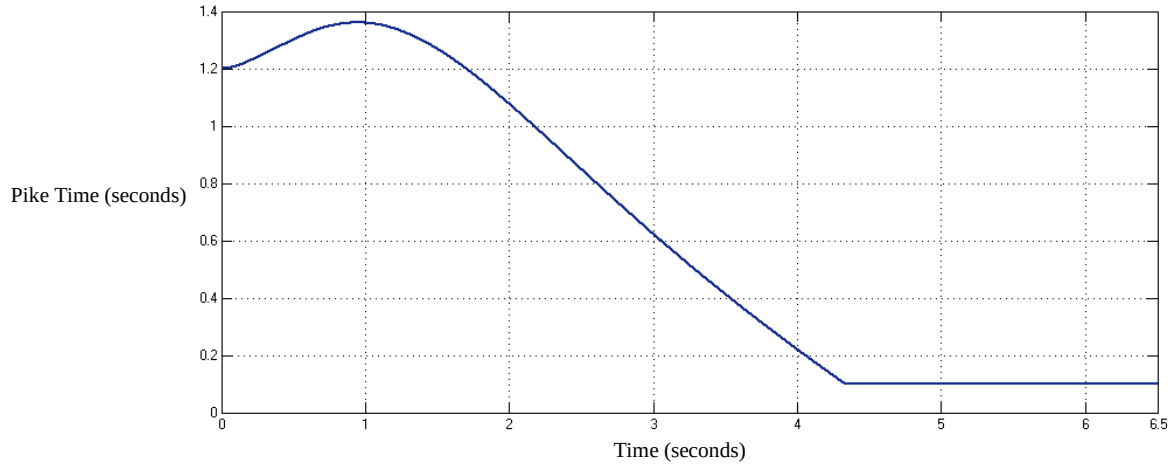

Figure 9 – Peak time possible to be developed by the actuator

The parameters for the desired dynamics are continuously calculated and thus the values of the controller gains can be determined at each processing step. The system gains are shown in Figure 10, 11 and 12 for the K_a, K_v and K_p, respectively.

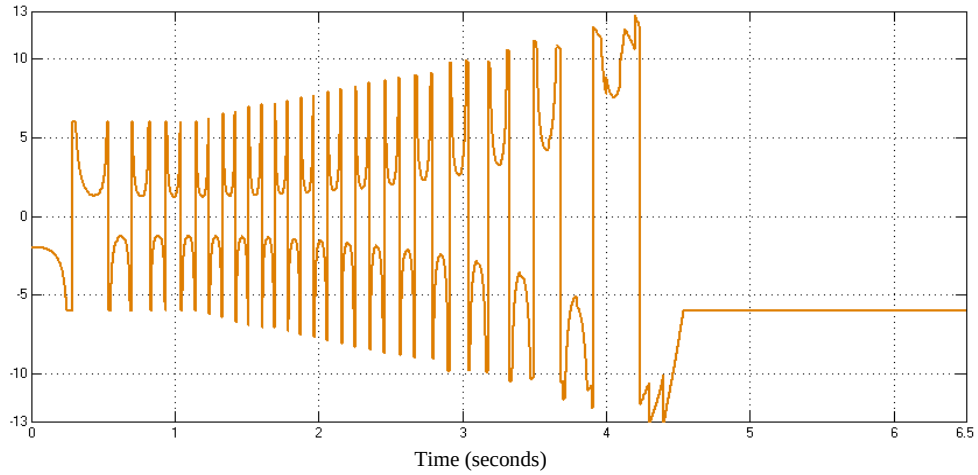

Figura 10 – Acceleration error gain K_a

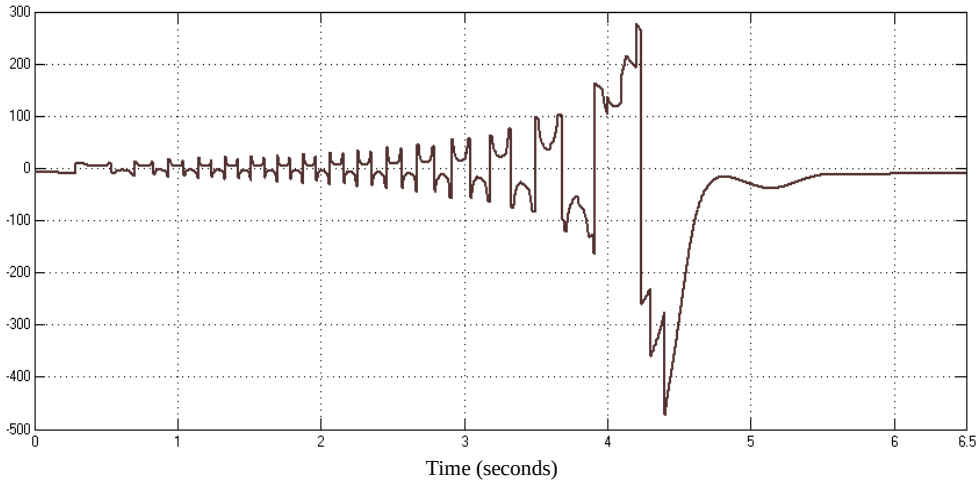

Figure 11 – Speed error gain K_v

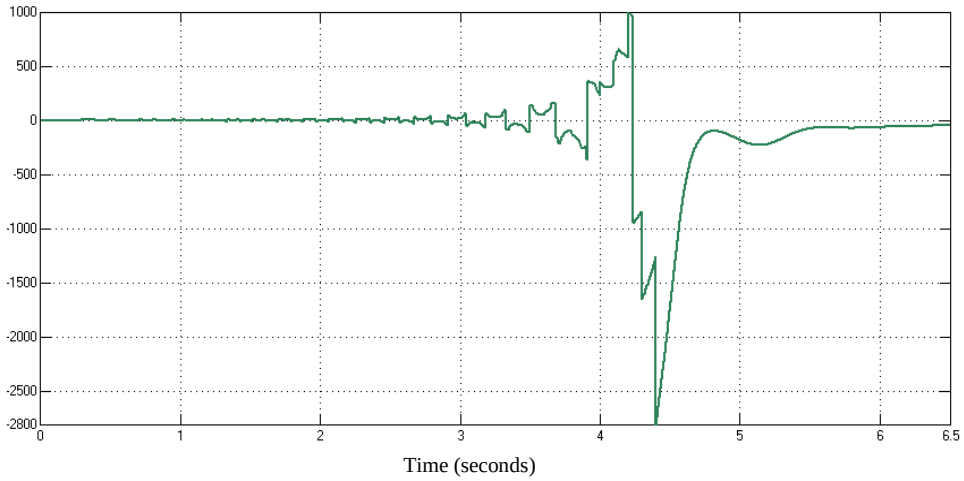

Figure 12 – Positioning error Gain K_p

From the analysis of Figures 10 to 12, it can be seen that in some moments the gains have a peak. This peak is explained due to the sine in the term A that is used to calculate these gains. When this senoid passes through the zero point, the terms tend to infinity, thus, as mentioned previously, the limitations in the gains imposed by the Lyapunov stability theory are used to adjust these parameters of the control and thus, these do not have very high values, which would provide electrical current peaks to the motor.

The gains of the control system multiplied by the system errors give rise to the control signal. As previously mentioned, this control signal must be multiplied by a gain (K_i) to transform into to electrical current and suit the

maximum allowed electrical current for motor performance. The gain K_i used was $1/22$. Figure 13 shows the electrical current that is transmitted to the motor by the control system.

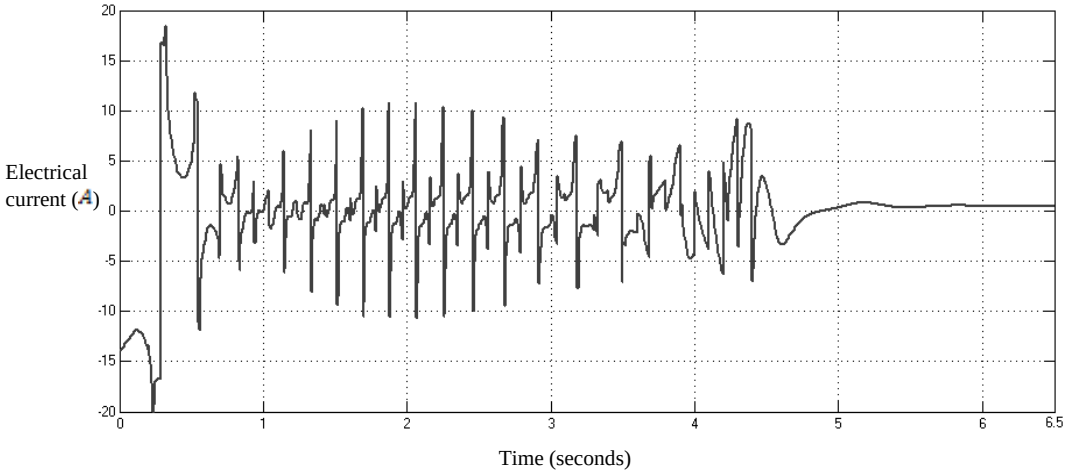

Figure 13 - Electrical current transmitted to the motor

The torque produced by the actuator, due to the electrical current passing through the phases, is shown in Figure 14.

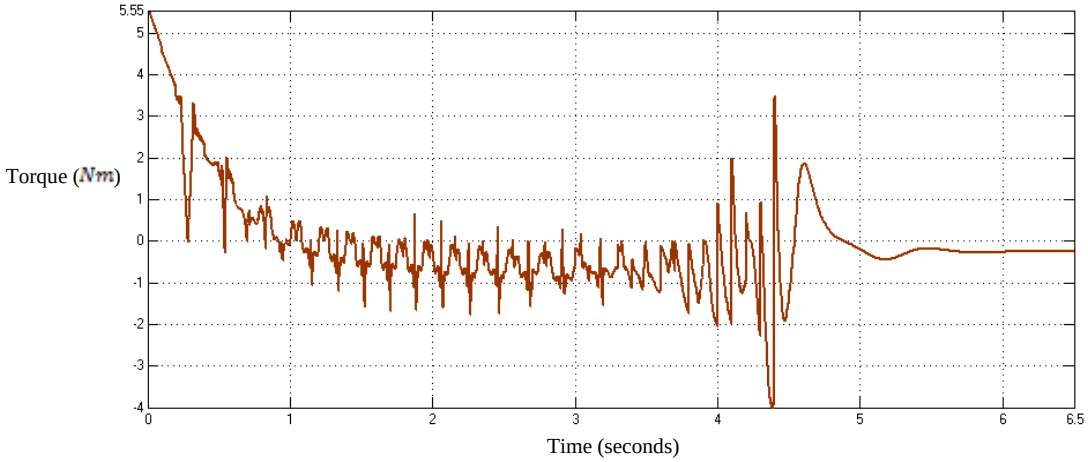

Figure 14 – Torque produced by the actuator

As can be seen from Figures 13 and 14, even after the stabilization of the motor, there is still electrical current supplied to the actuator and torque being produced.

This happens due to the actuator retention torque, in which, even when stopped, this torque tends to move the motor shaft (rotor), thus producing a small error in the acceleration, and because of this, the torque produced by the actuator tries to stabilize the acceleration error and counterbalance the retention torque. Figure 15 shows the retention torque produced during the simulation.

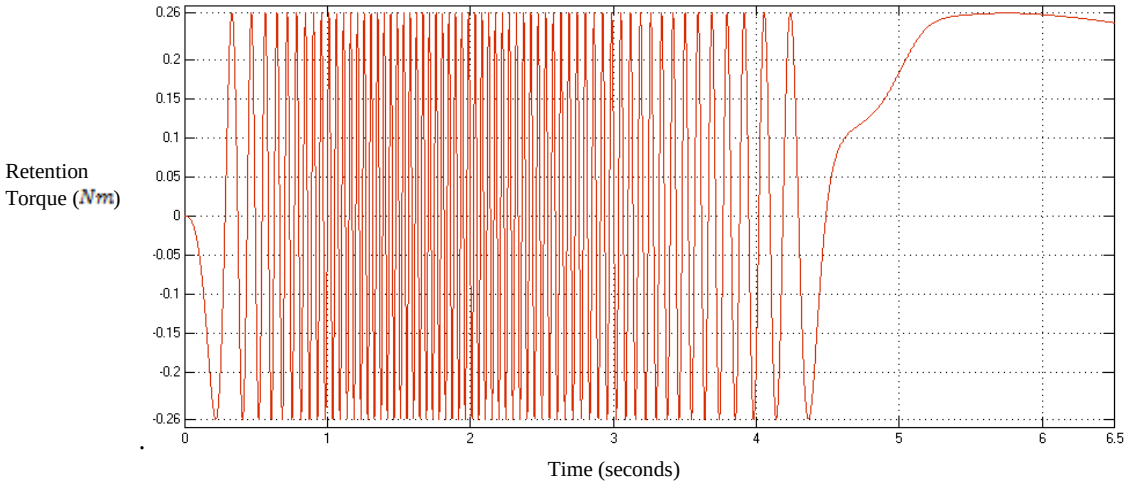

Figure 15 – Retention torque produced in the actuator

Figure 16 shows the actuator acceleration error as the actuator shaft moves to the required point, and, as shown in this figure, the acceleration error is practically zero after stabilizing the motor in the required position.

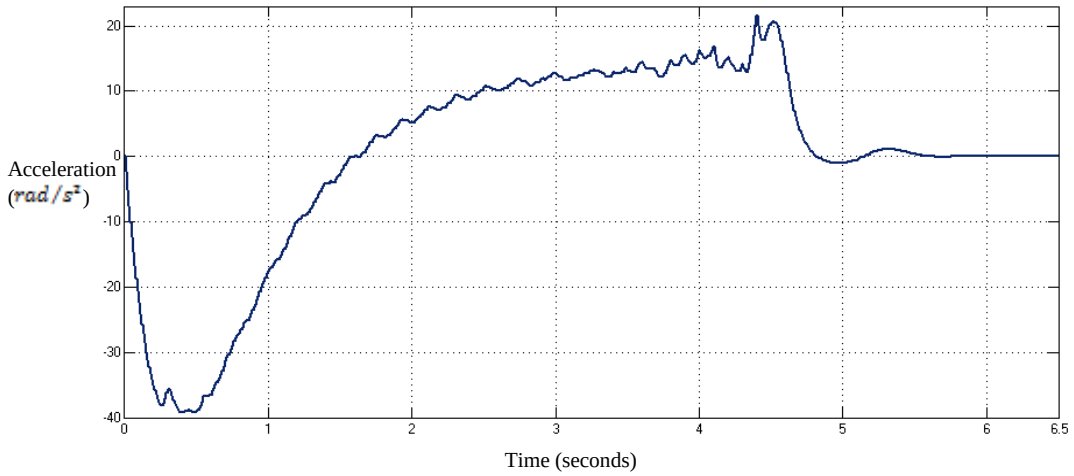

Figure 16 – Actuator acceleration error

Figure 17 focuses on the last moments of the simulation to facilitate the visualization of the acceleration error after reaching the required point.

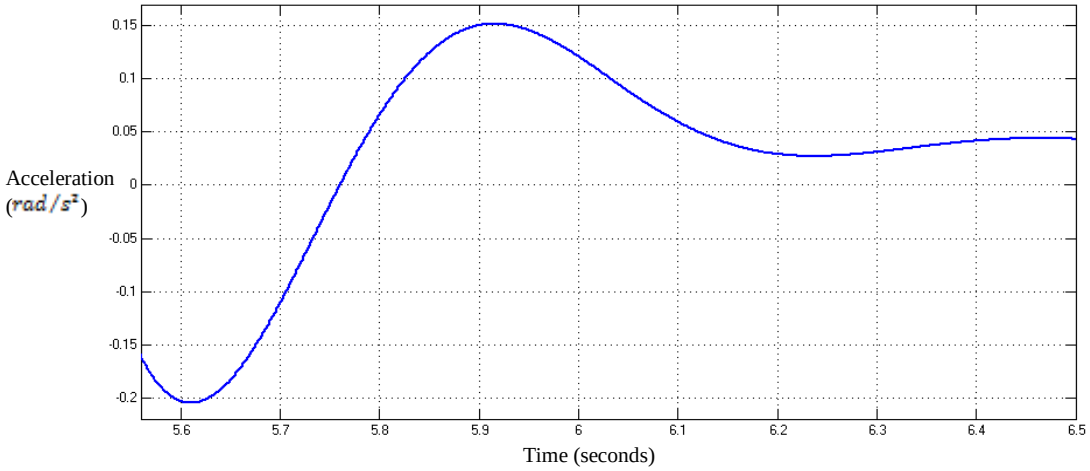

Figure 17 – Actuator acceleration error due to the retention torque

Finally, to demonstrate control efficiency, the speed error is shown in Figure 18, showing a virtually zero error after the actuator has found the required position.

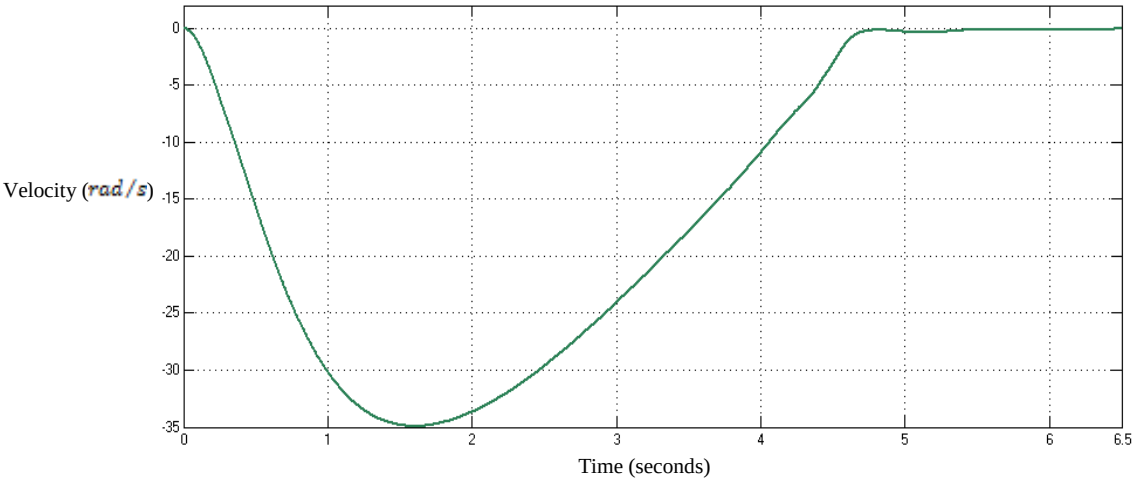

Figure 18 – Motor velocity error

4.2 Comparation with fixed PID controller

The first simulation performed is the point-to-point movement, shown in Figures 19 and 20, relative to the stepping motor control with fixed gains and varied gains, respectively. Table 3 shows the gains of the fixed PID control.

Table 3 - Gains of the fixed PID control

Gains	Values
K_p	110
K_v	41,22
K_a	3,19

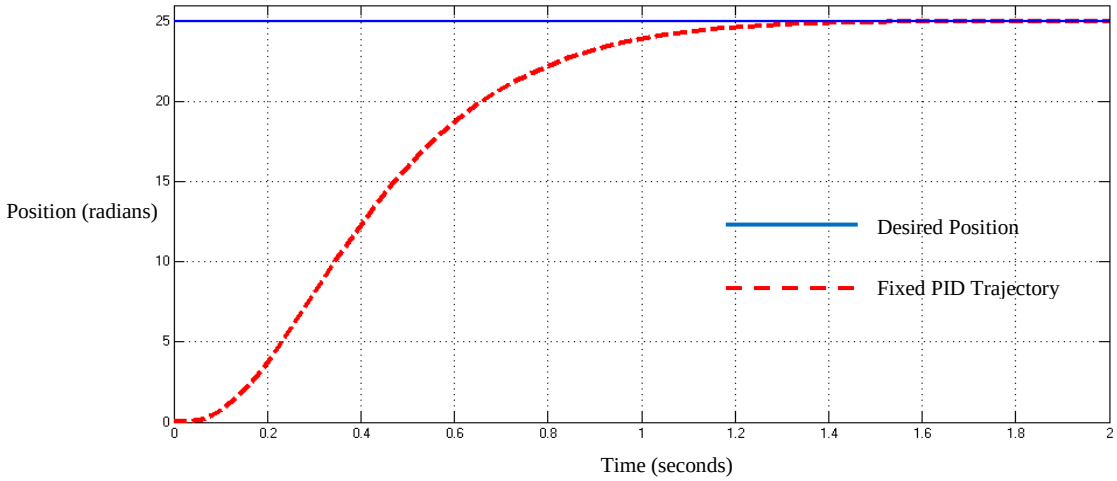

Figure 19 - Point-to-point movement for PID control with fixed gains

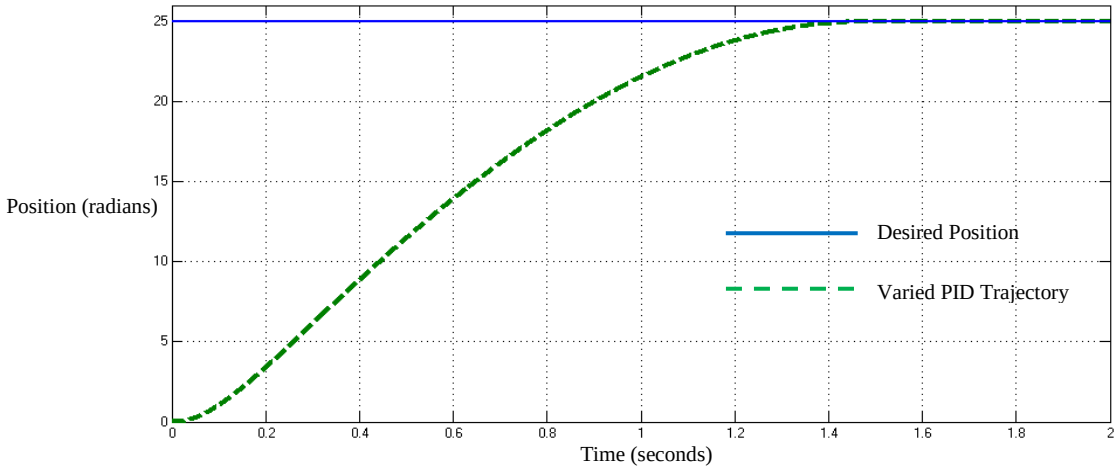

Figure 20 - Point-to-point movement for PID control with varied gains

As can be observed in Figures 19 and 20, the two controls reach the desired point of 25 radians, but the curve executed by the stepper motor with the proposed control is smoother, with fewer changes of trajectory, which causes less oscillations. This type of curve is desired because the main applications of these actuators are the positioning of components such as CNC machines and robotic manipulators.

For the trajectory tracking test, two trajectories were used, one with small displacement and one with similar displacement to the point-to-point test. The simulations of the first trajectory are shown in Figures 21 and 22 while the second test is presented in Figures 23 and 24, for the PID control with fixed gains and with variable gains, respectively.

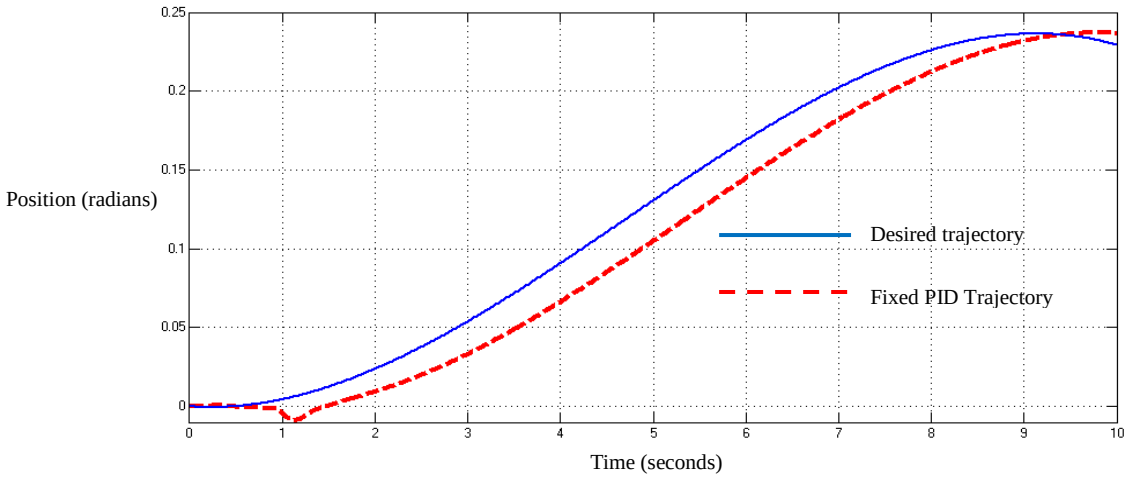

Figure 21 – First trajectory tracking for PID control with fixed gains

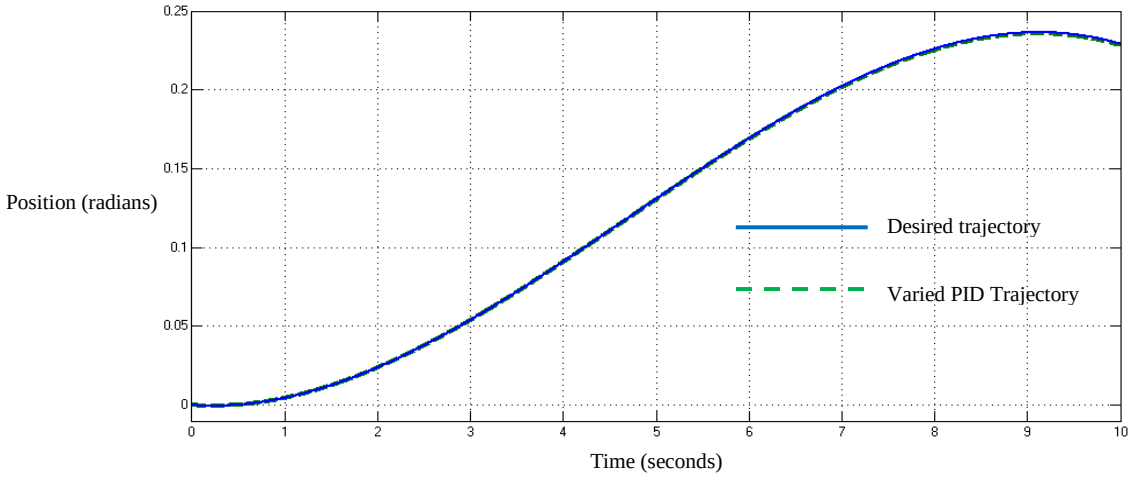

Figure 22 - First trajectory tracking for PID control with varied gains

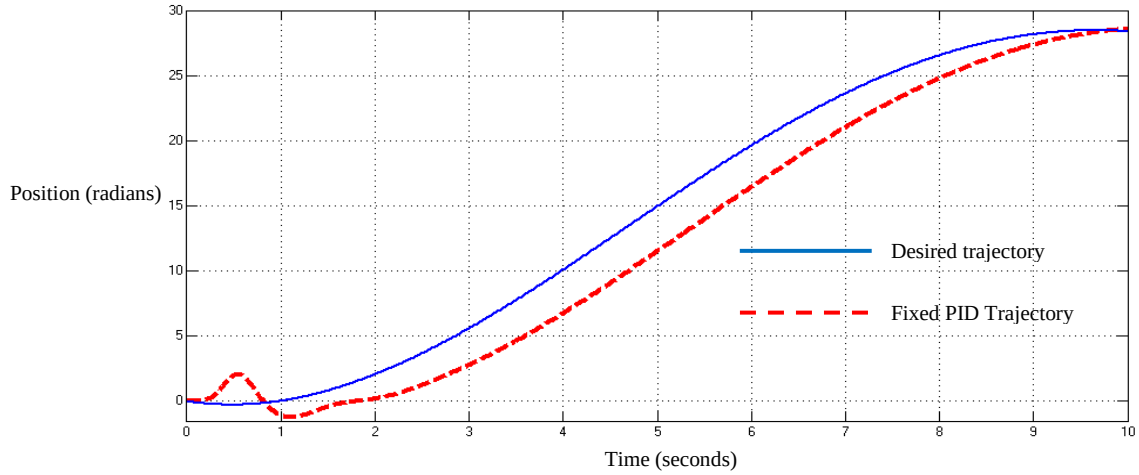

Figure 23 - Second trajectory tracking for PID control with fixed gains

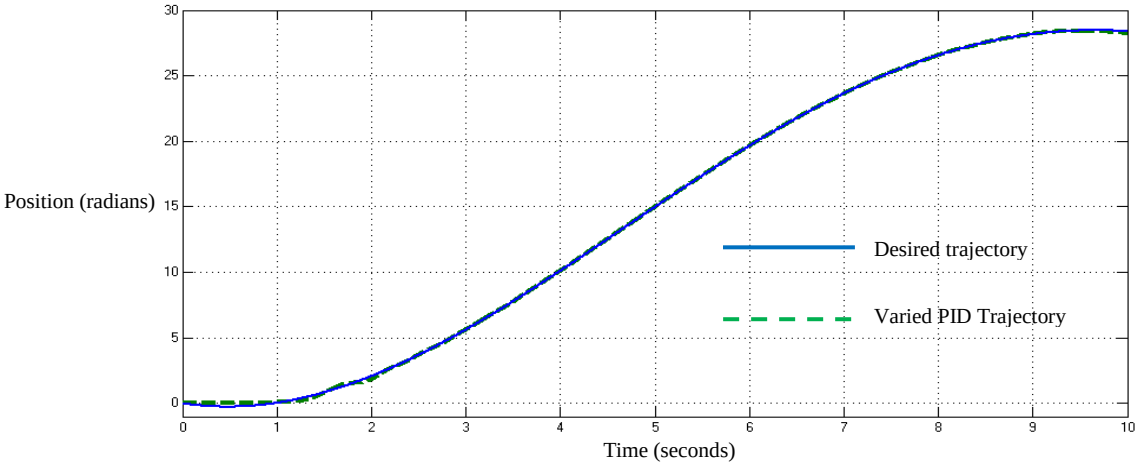

Figure 24 - Second trajectory tracking for PID control with varied gains

Table 4 shows the maximum errors found in each control tested for the two simulated trajectories.

Table 4 - Maximum errors in each control tested for the two simulated trajectories

Maximum trajectory error	Trajectory 1	Trajectory 2
Fixed PID	0,03 radians	2,4 radians
Variable PID	0,007 radians	0,3 radians

As can be seen from the analysis of Figures 21 to 24 and the results shown in Table 4, in addition to the oscillations and instability demonstrated mainly at the beginning of the trajectories for the PID control with fixed gains, the PID control with variable gains follows the trajectory more precise and with smaller errors when compared to the PID with fixed gains.

It is concluded that the proposed control is more efficient in the tests of point-to-point movement and trajectory tracking than a PID control with fixed gains, besides having a guarantee of stability. Thus, for the control of equipment that requires reliability and precision the proposed control can be used.

5. CONCLUSIONS

In the first section of Chapter 4, it is proven that the variable gain PID control is able to execute with precision and effectiveness the control of the point-to-point movement for the stepper motor, besides it guarantee a smooth movement curve and respecting the limitations of the actuator. Since the point-to-point movement is the type of operation most used in these actuators and the one that most requires of the motor capacity, it can be concluded that the PID control with varied gains presented in this work is adequate for the motor control.

It is added that, due to the comparisons with the PID control of fixed gains, the proposed control was more precise, it is justified by the greater smoothness of the curves executed for the point-to-point movement, by the precision obtained in the tracking trajectory test and by the results presented in Table 4.

In this way, the control proposed in this paper is effective for the control of stepper motors, even when the requirement of precision, speed of operation and utilization of the torque capacity are demanded.

6. REFERENCES

Acarnley, P. 2002. *Stepping Motors – A guide to theory and practice*; London: The Institution of Electrical Engineer, Fourth edition.

Akiyama, 2008, "AK85H/3.75-1.8 Stepper motor specifications", 20 Sep. 2017 < http://www.guiacnc.com.br/projetos-de-usuarios/minha-cnc-parte-eletroeletronica-wagner/?action=dlattach;attach=33019>.

Allgayer, R.S. 2011, *Desenvolvimento de um manipulador robotico cilindrico acionado pneumaticamente*, Masters dissertation, Porto Alegre, Brazil.

Borges, 2017, *Controle em cascata de um atuador hidráulico utilizando redes neurais*, Ph.D thesis. Porto Alegre, Brazil.

Cao, L. and SCHWARTZ, H.M. 1999, "Oscillation, Instability and Control of Stepper Motors", *Kluwer Academic Publishers: Nonlinear Dynamics* 18: 383–404.

Cardozo, W.S. 2012. *Controle de motores de passo aplicado a um manipulador robótico*; Masters dissertation; Rio de Janeiro, Brazil .

Carrillo-Serrano, R.V. Hernández-Guzmán, V. M. and Santibáñez, V. 2014, "Global asymptotic stability of pd control for pm stepper motor servo-systems". *Asian Journal of Control*, Vol. 16, No. 3, pp. 1–9.

Elksasy, M.S.M.; Gad, H.H. 2015. "A New Technique for Controlling Hybrid Stepper Motor Through Modified PID Controller"; *International Journal of Electrical & Computer Sciences, IJECS-IJENS* Vol:10 No:02. p28-35.

Kabde, A.B.; Savio, A.D.; "Position Control of Stepping Motor"; *International Journal of Advanced Research in Electrical, Electronics and Instrumentation Engineering*, p8974-8981.

Kamalasadan, S. 2007, "A New Intelligent Controller for the Precision Tracking of Permanent Magnet Stepper Motor"; *Power Engineering Society General Meeting*, p1-7; 24-28.

Machin, S. 2017, *Diseño de un controlador para un vehículo movil*, Masters dissertation, Porto Alegre, Brazil.

Mayé, P. 2016. *Moteurs Électriques Pour La Robotique*; Dunod, Paris, Third Edition.

Ogata, 1997, *Modern Control Engineering*, Prentice Hall, New jersey, Third Edition.

Rachid, A. 2006, "A Lyapunov Approach for the Tracking Control of a permanent magnet stepper motor" *Multiconference on "Computational Engineering in Systems Applications"(CESA)*, October 4-6, 2006, Beijing, China.

7. RESPONSIBILITY NOTICE

The authors are the only responsible for the printed material included in this paper.